This is a preprint, the final version is subject to change, of the American Mineralogist (MSA)
Cite as Authors (Year) Title. American Mineralogist, in press.
DOI: https://doi.org/10.2138/am-2020-7257

Revision 1

Micro- and Nano-Size Hydrogarnet Clusters in Calcium Silicate Garnet: Part II. Mineralogical, Petrological and Geochemical Aspects

Charles A. Geiger[*,1] and George R. Rossman[2]

[1] Department of Chemistry and Physics of Materials
Section Materials Science and Mineralogy, Salzburg University
Jakob Haringer Strasse 2a
A-5020 Salzburg, Austria

[2] Division of Geological and Planetary Sciences
California Institute of Technology
Pasadena, CA 91125-2500, USA

*Corresponding author
Tel. (0431) 662-8044-6226
E-mail: ca.geiger@sbg.ac.at

Revised version submitted to American Mineralogist: XX.XX.XX

This is a preprint, the final version is subject to change, of the American Mineralogist (MSA)
Cite as Authors (Year) Title. American Mineralogist, in press.
DOI: https://doi.org/10.2138/am-2020-7257

ABSTRACT

The nominally anhydrous, calcium-silicate garnets, grossular - $Ca_3Al_2Si_3O_{12}$, andradite - $Ca_3Fe^{3+}{}_2Si_3O_{12}$, schorlomite - $Ca_3Ti^{4+}{}_2(Si,Fe^{3+}{}_2)O_{12}$, and their solid solutions can incorporate structural OH^-, often termed "water". The IR single-crystal spectra of a number of calcium silicate garnets were recorded between 3000 and 4000 cm^{-1}. Spectroscopic results are also taken from the literature. All spectra show various OH^- stretching modes between 3500 and 3700 cm^{-1} and they are analyzed. Following the conclusions of Part I of this study, the garnets appear to contain local microscopic- and nano-size $Ca_3Al_2H_{12}O_{12}$- and $Ca_3Fe^{3+}{}_2H_{12}O_{12}$-like clusters dispersed throughout an anhydrous garnet "matrix". The substitution mechanism is the hydrogarnet one, where $(H_4O_4)^{4-} \Leftrightarrow (SiO_4)^{4-}$, and various local configurations containing different numbers of $(H_4O_4)^{4-}$ groups define the cluster type. A single (H_4O_4) group is roughly 3 Å across and most (H_4O_4)-clusters are between this and 15 Å in size. This model can explain the IR spectra and also other experimental results. Various hypothetical "defect" and cation substitutional mechanisms are not needed to account for OH^- incorporation and behavior in garnet. New understanding at the atomic level into published dehydration and H-species diffusion results, as well as H_2O-concentration and IR absorption-coefficient determinations, is now possible for the first time. End-member synthetic and natural grossular crystals can show similar OH^- "band patterns", as can different natural garnets, indicating that chemical equilibrium operated during their crystallization. Under this assumption, the hydrogarnet-cluster types and their concentrations can potentially be used to decipher petrologic (i.e., *P-T-X*) conditions under which a garnet crystal, and the rock in which it occurs, formed. Schorlomites from phonolites contain no or very minor amounts of H_2O (0.0 to 0.02 wt. %), whereas Ti-bearing andradites from chlorite schists can contain more H_2O (~0.3 wt. %). Different hydrogarnet clusters and concentrations can occur in metamorphic grossulars from Asbestos, Quebec, Canada. IR absorption coefficients for H_2O held in hydrogrossular- and hydroandradite-like clusters should be different in magnitude and this work lays out how they can be best determined. Hydrogen diffusion behavior in garnet crystals at high temperatures is primarily governed by the thermal stability of the different local hydrogarnet clusters at 1 atm.

Key words: Andradite, grossular, schorlomite, nominally anhydrous minerals, hydrogarnet clusters, IR spectroscopy, H_2O, metamorphism

INTRODUCTION

In Part I (Geiger and Rossman this volume) of this work it was proposed that micro- to nanosized hydrogrossular- and hydroandradite-like clusters can be found in the nominally anhydrous garnets grossular, andradite and their solid solutions. The discussion, therein, concentrated largely on analyzing the vibration behavior of the OH^- dipole and its spectroscopic nature, assigning various OH^- stretching modes observed in IR spectra and constructing a local crystal-chemical cluster model for garnets within the compositional system $Ca_3Al_2Si_3O_{12}$-$Ca_3Fe^{3+}{}_2Si_3O_{12}$-$Ca_3Al_2H_{12}O_{12}$-$Ca_3Fe^{3+}{}_2H_{12}O_{12}$. In this Part II, the focus of our research is more applied and we concentrate our efforts on different mineralogical, petrological and geochemical aspects of the new findings and proposals. Original scientific understanding is obtained because the cluster model explains IR spectra and, furthermore, permits an atomistic interpretation of many varied experimental results obtained on the nature of "water" in various calcium silicate garnets over many years. The amount of data and results that are available is wide ranging. Considerable and diverse research has been undertaken on OH^--bearing garnets over the last approximate three decades. And, here, it should be noted that in terms of the many grossular samples that have been studied by IR spectroscopy, that we are not aware of any "water"-free crystals. Much has been learned, but much is still not understood. What has been done?

In short, there has been: i) A number of analytical compositional, diffraction and spectroscopic studies undertaken that describe the structural and crystal-chemical properties of many various calcium silicate garnets (see references in Part I and this work), ii) Experimental studies have been made to determine hydrogen or hydrogen-species diffusion (and deuteration) behavior in both grossular (Kurka et al. 2005; Reynes et al. 2018) and andradite (Zhang et al. 2015) crystals following heating, and iii) Investigations have been made to determine H_2O

concentrations in grossular and in determining its IR absorption coefficient (Rossman and Aines 1991; Maldener et al. 2003; Reynes et al. 2018).

It turns out that all these studies were hampered, greatly or in part, though, because it was not understood how H^+ or OH^- was incorporated in the garnets being studied. It was generally assumed that "defects" and various coupled-chemical-substitution mechanisms controlled hydrogen incorporation in calcium silicate garnets. The cluster model introduced in Part I allows new interpretations and understanding on IR spectra, proton order, hydrogen-diffusion and H_2O concentration determinations. Moreover, first petrological and geochemical implications and conclusions can be drawn from IR spectra of different calcium silicate garnets and the types and concentrations of the clusters that they contain.

SAMPLES AND EXPERIMENTAL MEASUREMENTS

The garnet samples investigated via IR spectroscopy for this study and in the past at CIT are described in Table 1. The experimental IR single-crystal measurements are described in Part I. Spectral results were curve fit using the WiRE program of Renishaw that is part of their Raman systems. Spectra with sloping baselines were first manually baseline-corrected using the Wire program.

RESULTS

Figures 1 through 5 show IR single-crystal spectra that are analyzed in this study. Supplementary Table 2 shows how the H_2O contents for the various garnets, as discussed below, were calculated. The amounts are also listed in Table 1. Table 3 summarizes the energies of OH^- stretching modes, greater than 3560 cm^{-1}, for various garnets at room temperature as well as their assignment to a given cluster type (see Part I - Figure 4). Supplementary Table 4 gives the crystal-chemical formulae of a number of Ti-bearing garnets (taken from Armbruster et al. 1998) that are discussed below.

DISCUSSION

The long quest to understand "water" in garnet: hydrogarnet clusters vs defects and coupled substitutional mechanisms

The analysis of Geiger and Rossman (2018), together with that in Part I of this investigation, provides a new basis for interpreting IR spectra and understanding OH^- incorporation in different calcium silicate garnet species. A sense of order and understanding is established from these two studies through a crystal-chemical and vibrational model analysis that provides a coherent explanation for many various IR spectroscopic observations.

It appears that OH^- incorporation in nominally anhydrous Ca silicate garnet largely occurs through various local hydrogarnet-like clusters. It is well known from synthesis experiments (Flint et al. 1941; Carlson 1956; Kobayashi and Shoji 1983; Dilnesa et al. 2014) and through calculations (Wright et al. 1994) that the hydrogarnet substitution, that is $(H_4O_4)^{4-} \Leftrightarrow (SiO_4)^{4-}$, is both structurally and energetically favorable in calcium silicate garnet. It is much more favorable than in other garnet species, for instance, almandine, pyrope, majorite, and spessartine. From this knowledge and our cluster-model analysis (Part I), "defect-type" mechanisms involving the garnet {X}- or [Y]-site such as $\{Ca^{2+} \Leftrightarrow 2H^+\}$ and $[Al^{3+} \Leftrightarrow 3H^+]$ to account for OH^- incorporation in grossular (e.g., Basso et al. 1984; Birkett and Trzcienski 1984; Basso and Cabella 1990) may not be as common as thought or even present. The same argue holds for the defect $(SiO_3OH)^{3-}$ in garnet (Andrut et al. 2002) or the "point defect" $\{Fe^{3+}H^+\}$ in andradite (Reynes et al. 2018). It is also not necessary to invoke the presence of "nonstandard" silicate garnet cations (e.g., Li^+, Na^+, B^{3+}) and various coupled substitution mechanisms, for example, $\{Li^+\text{-}H^+ \Leftrightarrow Ca^{2+}/Mg^{2+}\}$, $[Mg/Fe^{2+}\text{-}H^+ \Leftrightarrow Al/Fe^{3+}]$, $(B^{3+}\text{-}H^+) \Leftrightarrow (Si^{4+})$, $[Fe^{3+}]\text{-}(H^+) \Leftrightarrow [Ti^{4+}]$, $(Al^{3+}\text{-}H^+) \Leftrightarrow (Si^{4+})$ to account for various observed OH^- bands in IR spectra of Ca-rich and other silicate garnets (e.g., Kühberger et al 1989; Khomenko et al. 1994; Lu and Keppler 1997; Reynes et al. 2018). The substitutions $H^+ + Al^{3+} \Leftrightarrow Si^{4+}$ and $H^+ + B^{3+} \Leftrightarrow Si^{4+}$, for example, do occur in other mineral structures (see review of Rossman 1986). However, we know of no scientific evidence or results, at this time, that could account for any of these different H^+ substitution mechanisms in garnet. We stress, though, that

our cluster-based model does not in any way exclude the possibility that other mechanisms could affect the nature of H^+ incorporation.

The scientific problem is challenging, because the precise stoichiometry and the possible occurrence of structural defects in silicate garnet are not understood. It is not known how exact silicate garnet stoichiometry is, namely $\{X_3\}[Y_2](Z_3)O_{12}$. Efforts are underway to make first headway in this regard (Geiger and Brearley in prep.). Another issue is that of garnet chemistry, and how it could affect OH^- incorporation. Moreover, the role of "nonstandard" cations and how they can substitute at $\{X_3\}$, $[Y_2]$ and (Z_3) and with different valence states in the common silicate garnets is still partly an open question. A good example is Ti^{4+}.

In Part I, the compositional system $Ca_3Al_2Si_3O_{12}$-$Ca_3Fe^{3+}{}_2Si_3O_{12}$-$Ca_3Al_2H_{12}O_{12}$-$Ca_3Fe^{3+}{}_2H_{12}O_{12}$ was considered and the nature of OH^- in these garnets analyzed. Of course, calcium silicate garnets can contain Ti^{4+}, which can occur in minor to major amounts. It is generally thought that the bulk of Ti occurs at [Y] (Locock 2008) and this, thereby, changes the local-charge-balance situation in the common silicate garnets. The presence of Ti^{4+} in calcium silicate garnet could determine how OH^- is incorporated. Kühberger et al. (1989) argued that the substitution $[Fe^{3+}] \Leftrightarrow [Fe^{2+}\text{-}H^+]$ occurs. Indeed, in terms of another garnet system, namely pyrope, and in both natural and synthetic crystals, the presence of Ti^{4+} appears to give rise to OH^- stretching bands located between 3510 and 3530 cm^{-1}. (Bell and Rossman 1992; Geiger et al. 2000). It follows that OH^- structural incorporation in pyrope is thereby affected. The IR spectra of Ti-bearing calcium silicate garnets need to be analyzed and compared to the spectra of garnets in the four component system given above.

Ti-containing calcium silicate garnets and their IR spectra

Andradite can contain significant amounts of Ti^{4+}. There are also calcium silicate garnet species with integral Ti^{4+}. Schorlomite, ideal end-member formula $\{Ca_3\}[Ti^{4+}{}_2](Si,Fe^{3+}{}_2)O_{12}$ and morimotoite $\{Ca_3\}[Ti^{4+},Fe^{2+}](Si_3)O_{12}$ are two such species. Furthermore, there are other Ti-

containing components that are used in formulations to calculate garnet crystal-chemical formulae (Locock 2008).

There have been a number of crystal-structure and mineralogical studies undertaken on Ti-bearing garnets, whose compositions and crystal chemistry can sometimes be complex (e.g., Locock et al. 1995; Armbruster et al. 1998; Chakhmouradian and McCammon 2005; Schingaro et al. 2016 and references therein). Briefly summarizing and stating the findings with regard to the goals of the research herein, there can be monovalent cations (e.g., Na^{+}) at {X}, Mg and Fe^{2+} at [Y], and Fe^{3+}, Al^{3+} and even Fe^{2+} can be found at (Z) as well as vacancies at the latter. Thus, the nature of structural OH^{-} could be affected through a number of various substitution mechanisms. What do the IR spectra of Ti^{4+}-bearing garnets show and how can they be interpreted?

The IR single-crystal spectrum of a Ti-bearing garnet, GRR 3554, from the well-known Magnet Cove locality, Arkansas, USA (Table 1) and its fit are shown in Figure 1. OH^{-} modes are present at 3529, 3563, 3582, 3605, 3620 and 3635 cm^{-1}. Following the OH^{-} mode assignments for garnets discussed in Part I (given in Table 3 of this work), the second and third modes in the list are assigned to hydroandradite-like clusters and latter three modes to hydrogrossular-like clusters. The OH^{-} mode at 3529 cm^{-1} has another origin and it will not be considered here. This goes for all modes located at wavenumbers below about 3560 cm^{-1}.

A number of IR single-crystal spectra on different Ti-bearing garnets and schorlomites have been published. The IR spectrum of a compositionally complex schorlomite, taken from the Ice River igneous alkaline complex, Yoho National Park, British Columbia, Canada, $\{Ca_{2.866},Mg_{0.08},Mn^{2+}_{0.019},Na_{0.038}\}_{3.003}(Ti^{4+}_{1.058},Zr^{4+}_{0.039},Al_{0.137},Fe^{3+}_{0.631},Fe^{2+}_{0.057},V^{3+}_{0.014},Mn^{3+}_{0.013},Mg_{0.055})_{2.004}[Si_{2.348},Fe^{3+}_{0.339},Fe^{2+}_{0.311},4H_{0.005}]_{3.003}O_{12}$, was measured by Locock et al. (1995). It shows a single, weak and broad asymmetric OH^{-} band with a maximum at 3563 cm^{-1} (this "band" can be simulated with three components). We interpret this as indicating that most of the OH^{-} is held in single, isolated $(H_4O_4)^{4-}$ groups of a hydroandradite-like cluster (Table 3). Kühberger et al. (1989) investigated the crystal chemistry and other properties of a natural schorlomite (Kaiserstuhl, FRG) and several synthetic Ti-bearing andradites. The IR spectrum of their synthetic

sample T-13, crystal-chemical formula $Ca_{2.98}[Fe^{3+}_{0.97},Fe^{2+}_{0.11},Ti^{3+}_{0.27},Ti^{4+}_{0.65}](Si_{2.38},Fe^{3+}_{0.32},Fe^{2+}_{0.12},Ti^{4+}_{0.16},4H_{0.3})$, shows two OH^- bands at 3568 and 3533 cm^{-1}. The former mode can be, once again, assigned to single, isolated $(H_4O_4)^{4-}$ groups of a hydroandradite-like cluster (Table 3). The amount of H_2O was given as 0.22 wt. % for this garnet synthesized hydrothermally at $P(H_2O)$ = 3 kbar and 750 °C. Schmitt et al. (2019) studied a number Ti-bearing andradites taken from a rodingite and presented a Raman spectrum on one garnet. It shows two overlapping OH^- bands with the most intense one located at 3568 cm^{-1}, once again, indicating the presence of an isolated hydroandradite-like cluster.

Armbruster et al. (1998) undertook a crystal-chemical study on a number of different natural Ti-bearing garnets using several experimental methods including IR single-crystal spectroscopy to measure OH^-. The formulae of these samples were calculated taking the microprobe results in Armbruster et al. (1998) and using the formulation of Locock (2008). The results are found in Supplementary Table 4. We analyze their IR spectroscopic results further (E. Libowitzky kindly provided the IR data from their work). The IR spectrum (Fig. 2) of the andradite sample, "Hilda", from a chlorite schist shows a complex OH^- band pattern with both weak and intense OH^- bands. A number of OH^- bands are located above 3560 cm^{-1} and they can be assigned to different hydrogarnet clusters, as given in Table 3. We think that the small differences in wavenumber compared to the equivalent modes observed in the spectra of grossular can be explained by differences in chemistry and cation masses between the two garnets (see discussion in Part I). We consider the overall agreement in OH^- wavenumbers to be, in general, good. As stated above, the nature of the OH^- modes located below about 3560 cm^{-1} is not fully understood at this time and this aspect requires more investigation.

It is notable that the amounts of OH^- contained in the different garnets is quite variable. A number of spectra from Armbruster et al. (1998) are plotted in Fig. 3, as is the spectrum for Ti-bearing andradite GRR 3554. All the samples are normalized to 1 mm thickness, allowing a simple comparison of OH^- mode wavenumbers and importantly, here, the relative OH^- amounts given by the mode intensities. Vertical lines are drawn to indicate the positions of the most intense

215 OH^- bands and, thus, the corresponding hydrogarnet cluster type. Consider, first, the relatively Ti-
216 poor grossular-andradite garnet, Mureia, that shows no H_2O in its core but some OH^- at its rim
217 (Fig. 3). This garnet, possibly from a serpentinite (Armbruster et al. 1998), apparently nucleated
218 and crystallized under low f_{H_2O} or even possibly dry conditions. At a later stage in metamorphism
219 and with further crystal growth f_{H_2O} increased, as the rim of the garnet contains OH^-. The *P-T*
220 phase relations of the system grossular-katoite ($Ca_3Al_2H_{12}O_{12}$) have been investigated (Yoder
221 1950; Pistorius and Kennedy 1960; Kobayashi and Shoji 1983) and they allow, together with the
222 IR results and our cluster model analysis, first petrological insight on OH^- in garnet. The phase
223 equilibrium results, as well as published synthesis data on hydrogarnets, show that the amount of
224 $Ca_3Al_2H_{12}O_{12}$ (and by assumption $Ca_3Fe^{3+}{}_2H_{12}O_{12}$ as well) in grossular is favored by lower
225 temperatures and is also a function of the f_{H_2O} of the system. Consider, second, the amounts of
226 H_2O in Ti-bearing garnets from different rock types. As an example, there are major differences in
227 H_2O amounts between schorlomites (i.e., samples KAlS and KB166) occurring in magmatic
228 phonolites vs garnets (i.e., samples ZER1 and HILDA) from lower-grade metamorphic rocks
229 containing chlorite. Garnets in the former crystallized under high temperatures ($T \geq 900$ °C) and
230 "dry" conditions (Braunger et al. 2018) compared to those occurring in chlorite schists, which
231 likely crystallized under H_2O-rich conditions and at $T < 500$ °C.

232 The amount of the H_2O in the different garnets shown in Fig. 3 can be calculated following
233 Rossman (2006) and are given in Supplementary Table 2. Some garnets contain very little H_2O
234 (sample KAlS 2 has 0.01 wt. % H_2O), while others contain more than an order of magnitude
235 greater concentration (sample ZER1 12 has 0.35 wt. % H_2O). We recognize that this analysis
236 involves garnets of different composition, but, nevertheless, we think the overall conclusion is
237 correct. We pursue the issue of hydrogarnet-cluster types and their concentration in a simple
238 petrologic context below with an analysis focused on nearly end-member grossular. But first, we
239 consider the physical and chemical nature of the various hydrogarnet cluster themselves.
240

241 **Micro- and nano-size hydrogarnet clusters and proton ordering**

We think, that with regard to OH^- incorporation in nominally anhydrous Ca silicate garnet, the term "hydrogarnet-like cluster" better describes the crystal-chemical situation than "OH^- defect". The latter term has been used, and sometimes in combination with different chemical substitution mechanisms, as discussed above. The term defect is deeply ingrained in the mineralogical literature. It can be interpreted as indicating that the H^+ atoms are not a stoichiometric and integral structural part of the garnet structure, that is, not described by crystallographic relationships. This is probably not the case. The nature of various hydrogarnet-like clusters in an anhydrous "garnet matrix" and their effect on the long-range crystal-structure symmetry remains to be clarified. Several novel structural and crystal-chemical aspects arise from this research.

First, what are the physical and chemical properties of the hydrogarnet-like-clusters considered herein? Our model analysis derives six hydrogarnet-like cluster types and a finite-sized katoite-like cluster. They are based on the number of $(H_4O_4)^{4-}$ groups in an immediate cluster (Fig. 4 - Part I). The clusters, themselves, may not be strictly ideal in terms of their atomic configurations and composition. Different local configurations for a given number of $(H_4O_4)^{4-}$ groups in a cluster around a YO_6 octahedron may exist and they cannot be determined from the IR spectra, at least at this time. Furthermore, the clusters could contain "defects" related to non-stoichiometry and proton order-disorder. The precise structural/crystallographic coordinates of the Ca cations at the Wyckoff position 24*c* and Al or Fe^{3+} cations at 16*d* in the clusters are probably slightly different than those for these atoms in the anhydrous garnet host. This should be the case because the Ca-O(1) and Ca-O(2) bond distances in the clusters and the anhydrous silicate garnet should be different, as they are between end-member katoite (Lager et al. 1987) and end-member grossular (Geiger and Armbruster 1997). It follows that there will be structural relaxation in the vicinity of a hydrogarnet cluster or clusters, but its exact nature will be difficult to determine via experiment.

The clusters give rise to proton ordering in the anhydrous host garnet and should, in a sense, introduce a type of short-range Ca ordering (see discussion in Palke et al., 2015, on short-

range cation ordering in garnet). It can be expected that variations in cluster spatial arrangements and $(H_4O_4)^{4-}$ group configurations will affect the nature of structural relaxation. This could lead to slight variations in OH^--mode energies (Table 3). In this regard, Geiger and Rossman (submitted - 2019c) have argued that minor amounts of OH^- in nearly end-member natural pyrope crystals are also held in hydrogrossular-like clusters. The OH^- mode energies associated with these clusters have slightly different wavenumbers than their mode equivalents in grossular garnet.

The precise nature of local structural and compositional heterogeneity, related to the presence of hydrogarnet clusters in a crystal, is subtle and not amenable to many types of experimental study. The clusters and structural heterogeneity probably cannot be detected by normal diffraction experiments. Possibly high-resolution TEM measurements could reveal something in this regard or maybe advanced MAS NMR experiments. In terms of composition, electron-microprobe or ion-probe measurements do not provide the necessary resolution to show the fine differences in local chemistry throughout a crystal.

The dimensions of the hydrogarnet-like-clusters cannot be determined experimentally from the IR spectra, but approximate dimensions of the $(H_4O_4)^{4-}$ clusters can be estimated from the models (Fig. 4 - Part I). The crystal structures of end-member andradite, grossular and end-member katoite are known well (Armbruster and Geiger 1993; Geiger and Armbruster 1997; Lager et al. 1987). The size of a single $(H_4O_4)^{4-}$ group is about 3 Å across (Fig. 4b - Part I). The size a $(H_4O_4)^{4-}$ cluster of the type shown in Fig. 4f (Part I) should be a little less than 10 Å, as measured from an outer $(H_4O_4)^{4-}$ to other $(H_4O_4)^{4-}$ group. A more extended, yet finite-size, katoite-like-cluster should have a minimum dimension of roughly 15 Å. Its exact upper size cannot be determined. Garnet, space group *Ia*-3*d*, has 8 formula units in its elementary cell and 24 crystallographic (Z) sites. This means 96 OH^- groups for hydrogarnet. Taking a garnet with a unit-cell roughly of size 12x12x12 Å (grossular has a unit-cell edge of 11.851 Å), gives a volume of 1,728 $Å^3$. The sizes of the various hydrogarnet-like-clusters are smaller than this or roughly similar. This puts the clusters on the lower end of the nanoscale.

Thermodynamic vs. kinetic considerations of cluster formation and stability

The hydrogarnet cluster model was constructed to account for and assign various OH^--stretching modes observed in the IR spectra of many different Ca-rich silicate garnets (Part I). The spectra and our analysis indicate that the cluster types can vary greatly from garnet to garnet with regard to their presence or absence as well their relative abundance. How is this to be interpreted? A key issue is whether the clusters were stable or metastable in a chemical thermodynamic sense during formation. If they were stable, a given hydrogarnet cluster must be a function of the pressure, temperature and composition (*P*-*T*-*X*) conditions of the system. This would mean that the cluster type(s) (i.e., OH^--richer vs. OH^--poorer clusters) must reflect the chemical and physical condition at which it nucleated and grew.

The IR spectra of grossular are quite diverse and complex with regards to this question (Part I), but information can be gleaned from the existing spectral library. Some crystals show the same OH^--band pattern from core to rim, while others show zoning reflected by changes in OH^--mode intensities. Crystals that are zoned with regard to their OH^--band patterns (i.e., cluster type variations), are reflecting changes in *P*-*T*-*X* during crystal growth, if they grew under chemical equilibrium. They could potentially be of use in determining how petrologic conditions evolved and changed in a metamorphic or igneous event. We explore this issue further.

At first glimpse, it may appear that the great range and diversity of IR spectra recorded on many different calcium silicate garnets could indicate that kinetic issues are operating during garnet crystallization. However, some sense of order and systematics can be observed in the myriad of spectra. Two examples are given by the garnets whose spectra are shown in Figures 3 and 6 in Part I.

In both cases there is a close resemblance in the IR spectra between a natural nearly end-member grossular and a synthetic hydrothermally grown crystal. The cluster types and their concentrations are similar for the two garnet pairs, thus, possibly indicating a stable chemical and structural state.

We examined, furthermore, the library of various natural grossular IR spectra measured in the lab of GRR to determine if similar OH^- mode patterns (i.e., cluster types) exist. Figure 4 shows the spectra of five garnets from various localities worldwide (Table 1). They can be described as grossular and grossular-andradite solid solutions with different $Al^{3+}/(Al^{3+} + Fe^{3+})$ ratios (i.e., ~0.05-0.07 for GRR 1422 and GRR 9456, ~0.22 for GRR 1424 and GRR 1429 and ~0.35 for GRR 1411). Indeed, their spectra are broadly similar in appearance with regard to their OH^- modes and, thus, the type of hydrogrossular-like and hydroandradite-like clusters. The main difference among the garnets lies in the amounts of the different cluster types. The broad likeness in the type of hydrogarnet clusters in various composition garnets from different localities lends credence to the argument that chemical equilibrium operated during their crystallization.

Hydrogarnet clusters and petrologic *P-T-X* conditions for grossular from a single geologic locality

The quarries located in or near Asbestos, Quebec, Canada are well known for producing different and excellent mineral specimens. Grossular crystals of different sizes (mm to cm) occur in this area with some closely approaching end-member grossular composition. Many are clearly of hydrothermal origin. Some crystals are colorless and transparent, while other are greenish, pink, orange, and pinkish-brownish in color. The origin of the color, which can be complex in nature, derives from the presence of small concentrations of transition metals (e.g., Fe^{2+}, Fe^{3+}, Cr^{3+}, Mn^{2+}, Mn^{3+}) located in the garnet structure.

The IR spectra of a number of different grossular samples from Asbestos are shown in Figure 5 and their OH^- band patterns vary considerably. The obvious question is why? Grossular crystals from Asbestos are typically found in rhodingites, associated with serpentinites, that experienced polymetamorphism. The geologic history of the area is complicated and evolved. Normand and Williams-Jones (2007) studied the petrology of the rocks and the *P-T* conditions of the different metamorphic events. All were relatively low grade in nature (e.g. 290-360 °C and 2.5-4.5 kbar for the first metamorphic event; 325-400 °C and less than 3 kbar for the second; and a

third, even lower-grade event occurring late in the geologic history). The fluid compositions operating during metamorphism were complex being moderately to highly saline and they contained methane.

The precise sample locations of the grossular crystals, whose spectra are shown in Figure 5, are not known, nor are the exact metamorphic periods of their crystallization. Three broad classes of spectra can be identified that reveal different hydrogarnet cluster types and their concentrations. They are: i) those garnets (i.e., samples 1538 and 1038) having both hydroandradite-like and hydrogrossular-like clusters with the latter having relatively abundant two and six $(H_4O_4)^{4-}$ groups as well as katoite-like clusters, ii) those garnets (i.e., samples 53b and 53RT) having hydrogrossular-like clusters characterized by relatively large amounts of three and four $(H_4O_4)^{4-}$ groups as well as katoite-like clusters, and iii) those garnets (i.e., samples 1537 and 1285 NMR) having hydrogrossular-like clusters characterized mostly by three $(H_4O_4)^{4-}$ groups. First, simple interpretations for the observations would suggest that group iii) grossulars crystallized at the highest temperatures and under high f_{H_2O} conditions, because more H_2O-rich clusters (Figs. 4a, e, f and g - Part I) should be the least stable thermally. Other grossulars from this group in Figure 5 crystallized perhaps at lower temperatures. Finally, the core of garnet 1038 may have crystallized at higher f_{H_2O} conditions than the rim (see discussion of andradite from Mureia in Fig. 3 above). More investigation is needed to determine if grossulars (different generations) with different hydrogarnet cluster types and concentrations can be explained in terms of their metamorphic history and *P-T-X* conditions.

Consider further the effect of temperature on the OH^- concentration in grossular. Fig. 6 in Part I is useful. Here, the spectra of a natural (GRR 1285 from Asbestos) and synthetic grossular (GR83) are compared and show two bands having similar energies of 3623 and 3604 cm^{-1}. The mode intensities in the two spectra, though, are greatly different. The spectrum of the synthetic crystal is based on 1 mm thickness, whereas the natural crystal, showing an expanded intensity of three, is for a crystal thickness of 0.03 mm. This means that the natural grossular crystal contains roughly 7 times more H_2O. The difference is likely related to the large difference in the

temperatures of crystallization between the two samples. Gr83 was synthesized at 1000 °C (Withers et al. 1998), whereas GRR 1285 from Asbestos likely crystallized at less than 400 °C.

It is important to note, here, that the discussion has considered small amounts (less than roughly 0.3 wt. % H_2O) of H_2O in nominally anhydrous garnets. True hydrogarnets, that is crystals with more than about 50 mole % hydrogarnet, can be found in nature (see introduction of Part I). Their temperatures of crystallization should be very low at $T < 300$ °C. Indeed, experiments on various composition silica-containing hydrogarnets show that they are not stable above 200 to 300 °C under hydrothermal conditions depending on their precise composition (Flint et al. 1941). Carlson (1956) gives the upper thermal stability under hydrothermal conditions for end-member katoite at roughly 225 °C. Grossular-rich grossular-katoite solid solutions (i.e., mole % grossular from 66 mole % to 100 mole %) are stable from 270/330 °C to 650 °C at $P_{H_2O} = 100$ Mbar with increasing stability with increasing grossular component (Kobayashi and Shoji 1983).

It could be argued, on the other hand, that the great variability in the observed OH^--band patterns for many different grossulars indicates that kinetics could have played a role in the formation and distribution of hydrogarnet-like-clusters in at least for some crystals. Consider the OH^--bond energies. One has 1.0 Joule = $5.034 \cdot 10^{22}$ cm^{-1}. Thus, 3600 cm^{-1} is equal to 43.1 kJ/mole and 10 cm^{-1} is equal to 0.12 kJ/mole. The difference in energy between, say, two OH^--modes at 3600 and 3611 cm^{-1} is only roughly 0.3 %. The energetics of chemical bonding associated with small amounts of OH^- are slight compared to the total bond energies in a crystal. This consideration could indicate that kinetic factors could play a role in the formation of clusters and that their presence represents metastability. This leads to the next question of H_2O concentrations in nominally anhydrous garnet.

Experimental investigations on the concentration of H_2O in calcium silicate garnet and absorption coefficient determinations for IR spectra: Consequences of the cluster model

Vibrational spectra, alone, do not suffice to determine the amounts of any chemical species. This requires first, in the general case, an independent experimental determination of

absolute H_2O concentrations and then, ultimately, a determination of IR absorption coefficients for OH^- modes can be made via a calibration. At this point, a spectrum suffices for an analytical determination of the amount of H_2O (see discussion in Rossman 2006). To start, the absorption coefficients for OH^- stretching modes in different phases and materials are different in magnitude depending on their wavenumber (Libowitzky and Rossman 1997). There have been several investigations related to determinations of H_2O contents in natural grossular crystals using IR spectroscopy in combination with diverse analytical methods (Rossman and Aines 1991; Maldener et al. 2003; Rossman 2006; Reynes et al. 2018 and works cited therein).

It can be expected that a general or averaged absorption coefficient describing all hydrogrossular clusters must be different than that for describing hydroandradite-like clusters. Moreover, because the various hydrogrossular cluster types are characterized by different energy OH^- modes, the IR molar absorption coefficients associated with each mode could be quantitatively different. How different or similar they are remains to be determined. It is notable that the published studies on absorption coefficient determinations often involved grossular-andradite garnets, whose IR spectra indicate both cluster types. Calibrations for H_2O in katoite(hydrogrossular) and grossular garnets (supplementary Table 2) are based on spectra having different energy OH^- modes. Moreover, some previously studied garnets (Maldener et al. 2003; Reynes et al. 2018) show high-energy modes in their spectra that are possibly related to the presence of OH^--bearing inclusion phases, as discussed in Part I (e.g., Fig. 8).

The spectral analysis, herein, sets out how absorption coefficient studies for H_2O should be undertaken. In concrete terms, for example, the "end-member" andradite 4282 (Part I - Table 1 and Fig. 11) would be unsuitable for a calibration study to obtain an absorption coefficient for H_2O in andradite garnets. On the other hand, samples such as GRR 53, 1537 and 1285 NMR (Fig. 5) would be suitable for determining H_2O contents in grossular.

H_2O loss in grossular and H^+ species diffusion behavior

The H_2O loss and hydrogen diffusion behavior in grossular and grossular-andradite garnets

have been investigated at ambient pressure after high-temperature treatment of single crystals in several investigations (Kurka et al. 2005; Phichaikamjornwut et al. 2011; Reynes et al. 2018). The conclusions drawn in this study permit the three published results to be reanalyzed.

The grossular-rich crystal used by Kurka et al. (2005) in their hydrogen mobility study had the composition $Gross_{83.2}Andr_{14.3}Pyr_{2.2}$. The IR single-crystal spectrum of their sample GRO5 showed intense OH^- bands at 3568, 3600, 3645 (most intense), 3657 and 3687 cm^{-1}. Additional shoulders on these bands were also observable. The diffusion study was undertaken by treating prepared crystal platelets in a stepwise manner at temperatures of 1073 (800 °C), 1173 (900 °C), 1223 (950 °C), 1273 (1000 °C) and 1323 K (1050 °C) at 1 atm in air and gas mixtures ($Ar-H_2/D_2$) for various time periods (0 to 48 h). Then, the IR spectra of the platelets were recorded and the intensity of the different modes measured. For example, the spectra of a crystal heated at 1273 K showed a decrease in intensity for all modes as a f(*t*) and after 22 hr. only the mode at 3645 cm^{-1} was still visible. Kurka et al. (2005) concluded, in short, based on these and other results on intensity changes, that at least two types of OH^- "defects" were present in their grossular crystal. We make other conclusions. We think that the mode at 3687 cm^{-1} is possibly related to tiny "serpentine mineral" inclusions. Thus, it could be expected to show a different temperature dependence compared any garnet-related OH^--mode. Furthermore, we assign, as discussed above, the mode at 3568 cm^{-1} to a single $(H_4O_4)^{4-}$ group in a hydroandradite-like cluster and those modes at 3600, 3645, and 3657 cm^{-1} to different hydrogrossular-like clusters (Table 3). The hydrogen diffusion behavior for the two types clusters should be different.

Phichaikamjornwut et al. (2011) investigated the thermal and dehydration/rehydration behavior of several different composition garnets across the grossular-andradite binary in a similar experimental manner. Garnets were treated at 1 atm in air or H_2 at 973 K (700 °C) to 1173 K (900 °C) for different time periods and then the intensities of the different OH^- modes were measured by IR spectroscopy. The natural untreated crystals showed five intense OH^--modes at 3600/2, 3612/3, 3631, 3641 and 3662 cm^{-1} in grossular-rich and intermediate composition garnets. They can be assigned to different hydrogrossular-like clusters (Fig. 4 - Part I). The spectra of andradite-

rich crystals showed, in comparison, strong OH^- modes at 3653 and 3581 cm^{-1} and can be assigned to two different hydroandradite-like-clusters. Less intense modes were also observed in the spectra, but are not considered here. This team of researchers, in line with the conclusions of Kurka et al. (2005), argued that at least two different OH^- "defects" were operating in their dehydration experiments. This conclusion was based, once again, on different mode intensity behavior between hydrogrossular-like-cluster related OH^--modes and hydroandradite-like-cluster OH^- modes. We reinterpret these results and assign the two "defect types", in a broad sense, to two different hydrogarnet-cluster types.

Reynes et al. (2018) investigated the hydrogen concentration and diffusion behavior in three different natural grossular (and spessartine as well) samples in a different experimental sense using IR single-crystal and ion-microprobe (SHRIMP-SI) methods. The latter was used to measure H_2O concentrations and to also make an absorbance coefficient calibration. The IR spectra of their grossular samples are consistent with those described herein. That is, the most intense OH^- bands above 3600 cm^{-1} can be assigned to different hydrogrossular clusters and those below to hydroandradite clusters and other presently unassigned modes. They observed a mode at 3687 cm^{-1} that is possibly related to tiny "serpentine mineral" inclusions. The diffusion experiments on grossular (composition $Gross_{91.0}Andr_{6.4}Almd_{1.6}Spess_{0.1}$) were carried out a prepared cube of 1.5 mm size that was treated at 1 atm at various temperatures, 750-1050 °C, and oxygen fugacity conditions for 1 h to 10 days. IR spectra and OH^- modes were recorded from sections taken from the core to the rim of the crystal cubes, thus, permitting H_2O concentration profiles to be determined. We summarize and reinterpret the extensive results of Reynes et al. (2018). They observed, for example, in the IR spectra that the OH^- mode at 3645 cm^{-1} changed the least in intensity versus those at 3686 (probably "serpentine" mineral phase), 3657, 3628 and 3604 cm^{-1} as a function of temperature and time from the core to the rim of the cube. The latter modes essentially disappeared, while the former remained relatively strong in intensity. This result agrees excellently with the experimental observations of Kurka et al (2005). It appears, therefore, that the hydrogrossular cluster of the type shown in Fig. 4f (Part I) is the most stable against elevated

temperatures. Moreover, Reynes et al. (2018) observed clear differences in the water concentration profiles associated with the OH^- modes at 3576, 3567 and 3533 cm^{-1} compared to those modes associated with hydrogrossular-like clusters. As before, the first two modes are probably related to hydroandradite-like clusters, while the latter lowest energy OH^- mode remains to be assigned. A question associated with all of these three investigations relates to how, in a crystal-chemical sense, the hydrogen atoms are lost from heat treated crystals.

The oxidation-reduction reaction:

$$Fe^{2+} + OH^- \Leftrightarrow Fe^{3+} + O^{2-} + 1/2H_2 \qquad (A)$$

has been considered in different studies to account for hydrogen loss or incorporation in various nominally anhydrous silicates and, here specifically, garnet at elevated temperatures (Kurka et al. 2005; Phichaikamjornwut et al. 2011; Reynes et al. 2018). This reaction would require the initial presence of Fe^{2+} presumably at [Y] to permit H_2 loss. Fe^{2+} is present in some Ti-bearing garnets (see discussion on schorlomite garnets), but its possible occurrence and concentration in andradite-grossular garnets is not understood. Phichaikamjornwut et al. (2011) could not identify octahedrally coordinated Fe^{2+} in their garnets, at least at the level given ^{57}Fe Mössbauer spectroscopy, and concluded that hydrogen exchange via (A) did not occur in the majority of their samples. Kurka et al. (2005) and Reynes et al. (2018), in contrast, were more amenable to the possibly of this redox reaction. Reaction mechanism (A) cannot, of course, operate, at least in a local atomic nearest-neighbor sense, for either a hydrogrossular- or a hydroandradite-like cluster.

The presence of Fe^{2+} versus Fe^{3+} at [Y], should affect the energy of an OH^- stretching mode via the vibrational system around an O^{2-} atom, as shown in Fig. 2 (Part I), because their charges and ionic radii are different (i.e., high spin $^{VI}Fe^{3+}$ = 0.65 Å and $^{VI}Fe^{2+}$ = 0.78 Å - Shannon 1976). Therefore, the strengths of their chemical bonding to O^{2-} must also be different and the vibrational energy of the OH^- dipole must be affected. The IR spectra of untreated vs. heated garnets do not, however, give any indication of a significant change in energy for any OH^--modes (Further discussion on the possibly of oxidation-reduction reactions in spessartine garnet are discussed in Geiger and Rossman in prep. – 2019d).

Based on all these considerations, we think that the published dehydration-"diffusion" results and conclusions drawn from them can be interpreted in an alternative manner. Under the assumption that garnet is stochiometric (i.e., 12 oxygen atoms), and where the substitution $(H_4O_4)^{4-} = (SiO_4)^{4-}$ or $(4H)^{+} = (Si)^{4+}$ occurs, a simple breakdown reaction may be occurring. The simplest reaction at 1 atm in air would be in terms of local hydrogarnet clusters and in a purely general manner:

$$Ca_3Al_2H_{12}O_{12} \Leftrightarrow Ca_3Al_2O_6 \text{ (tricalcium aluminate)} + 6H_2O \quad \text{(B)}$$

and

$$Ca_3Fe^{3+}{}_2H_{12}O_{12} \Leftrightarrow Ca_3Fe^{3+}{}_2O_6 \text{ (tricalcium ferrite)} + 6H_2O \quad \text{(C).}$$

The back reactions of (B) and (C) occur in the crystallization of certain cements. End-member katoite breaks down at about 300 °C at 1 atm in air as based on TGA and DTA measurements (Dilnesa et al. 2014). This temperature is much lower than those at which dehydration/diffusion experiments were made (Kurka et al. 2005; Phichaikamjornwut et al. 2011; Reynes et al. 2018). Alternatively, the breakdown products of the clusters could be a poorly crystalline or amorphous material, as Belyankin and Petrov (1941) reported an endothermic reaction of hibschite to possibly an amorphous material at 650-690 °C at 1 atm in air.

The dehydration behavior of synthetic garnets of composition $Ca_3Al_2(SiO_4)_y(OH)_{4(3-y)}$ ($0 < y < 0.176$) was investigated *in situ* using neutron thermodiffractometry (Riva-Mercury et al. (2008)). The results and interpretations are too extensive to discuss fully here. Suffice it to say, that $Ca_3Al_2H_{12}O_{12}$ broke down slightly above 300 °C to mayenite [$Ca_{12}Al_{14}O_{32}(OH)$] and $Ca(OH)_2$ with the latter reacting to CaO and H_2O above 540 °C. The situation involving SiO_2-bearing $Ca_3Al_2(SiO_4)_y(OH)_{4(3-y)}$ garnet is more complex. In short, the anhydrous assemblage $Ca_{12}Al_{14}O_{33}$ + $n Ca_3SiO_5$ + mSiO2 may ultimately form at elevated temperatures (Riva-Mercury et al. 2008).

Concluding this discussion, experimental investigation is required to determine how local hydrogarnet clusters behave (i.e., their stability) in nominally anhydrous garnet at elevated temperatures.

538 **Hydrogen diffusion and deuteration behavior in andradite**

539 Zhang et al. (2015) researched the kinetic behavior of the deuteration process in andradite
540 garnet following treatment at elevated temperatures and 1 atm to remove the hydrogen atoms.
541 Their garnet sample, used for study, was close to "end-member" andradite composition and its IR
542 spectrum is similar in appearance to that shown in Fig. 9 – Part I with OH^- bands at 3634, 3612,
543 3583 and 3564 cm^{-1} with the latter three being strong in intensity. It follows that the garnet has
544 both hydrogrossular- and hydroandradite-like clusters. An analysis of the behavior of hydrogen
545 loss and deuterium gain was based on the intensity behavior of two curve-fitted OH^- modes at
546 3628 and 3634 cm^{-1} (and their OD^- equivalents at 2677 and 2680 cm^{-1}). These modes were derived
547 from a spectral deconvolution producing 12 OH^- bands, a number of which are strongly
548 overlapping, of the experimental IR spectra. Because of the spectral complexity, a precise
549 interpretation of their results using our cluster model is difficult to make. However, based on the
550 experimental spectra and an analysis of the behavior of the three most intense bands at 3612, 3583
551 and 3564 cm^{-1}, it appears that the deuteration process is more extensive for the andradite-like
552 clusters (bands at 3583 and 3564 cm^{-1}) compared to the most prevalent hydrogrossular-like cluster
553 (band at 3612 cm^{-1}).

554 Finally, Zhang et al. (2015) conclude from their results that H diffusion in andradite is
555 more than two orders of magnitude faster than in the case for grossular. One can argue that
556 hydrogrossular-like clusters in grossular are more stable than hydroandradite-like clusters in
557 andradite at elevated temperatures. This proposal is consistent with the synthesis experiment
558 results on the grossular-katoite and andradite-$Ca_3Fe^{3+}{}_2H_{12}O_{12}$ binaries (see Part I) that show that
559 solid solution is more complete in the former binary than in the latter. Of the various possible
560 hydrogarnet components in Ca silicate garnet, the hydrogrossular one appears to be the most
561 structurally and energetically favorable.

562

563 **IMPLICATIONS**

What are the mineralogical, petrological and geochemical consequences and implications following from this investigation? First, there has been considerable research done to determine the concentration of "H_2O" in garnet because of its global geochemical and geophysical significance for both crustal and deep mantle rocks. We think a determination of H_2O contents via IR spectroscopy will depend on what type of cluster the OH^- is held in calcium silicate garnets and especially between hydrogrossular-like and hydroandradite-like clusters. It needs to be researched what the general or averaged IR absorption coefficients for both types of clusters are.

Second, the question of thermodynamic or kinetic (metastable) behavior of cluster formation needs study. If chemical equilibrium was operating during cluster nucleation and growth, then "water" concentration in garnet is a function of the *P-T-X* conditions during crystallization and especially f_{H_2O}. It remains to be fully determined if and when the different cluster types and their amounts, as well as their spatial distribution throughout a crystal, reflect the *P-T-X* conditions during garnet growth. The partitioning of H_2O between hydrogrossular-like and hydroandradite-like clusters also needs to be determined for a range of garnet compositions.

ACKNOWLEDGMENTS

Dr. E. Libowitzky (Vienna) kindly provided IR data for the Ti-bearing garnets from the study of Armbruster et al. (1998). This research was supported by grants from the Austrian Science Fund (FWF: P 30977-NBL) to C.A.G. and the NSF (EAR-1322082) to G.R.R. C.A.G. also thanks the "Land Salzburg" for financial support through the initiative "Wissenschafts- und Innovationsstrategie Salzburg 2025". Dr. H. Skogby (Stockholm) and Dr. K. Wright (Perth) made constructive comments that improved the manuscript.

REFERENCES

Andrut, M., Wildner, M., and Beran, A. (2002) The crystal chemistry of birefringent natural uvarovites. Part IV. OH defect incorporation mechanisms in non-cubic garnets derived from polarized IR spectroscopy. European Journal of Mineralogy, 14, 1019-1026.

Armbruster, T., Birrer, J., Libowitzky, E. and Beran, A. (1998) Crystal chemistry of Ti-bearing andradite. European Journal of Mineralogy, 10, 907-921.

Allen, F.M. and Busek, P.R. (1988) XRD, FTIR, and TEM studies of optically anisotropic grossular garnets. American Mineralogist, 73, 568-584.

Basso, R. and Cabella R. (1990) Crystal chemical study of garnets from metarodingites in the Voltri Group metaophiolites (Ligurian Alps, Italy). Neues Jahrbuch für Mineralogie – Monatshefte, 3, 127-136.

Basso, R. Cimmino, F., and Messiga, B. (1984) Crystal chemistry of hydrogarnets from three different microstructural sites of a basaltic metarodingite from the Voltri Massif (Western Liguria, Italy). Neues Jahrbuch für Mineralogie – Abhandlungen, 148, 246-258.

Bell, D.R. and Rossman, G.R. (1992) The distribution of hydroxyl in garnets from the subcontinental mantle of southern Africa. Contributions to Mineralogy and Petrology, 111, 161-178.

Birkett, T.C. and Trzcienski, Jr., W.E. (1984) Hydrogarnet: Multi-site hydrogen occupancy in the garnet structure. Canadian Mineralogist, 22, 675-680.

Belyankin, D.S. and Petrov, V.P. (1941) The grossularoid group (hibschite, plazolite). American Mineralogist, 26, 450-453.

Braunger, S., Marks, M.A.W., Walter, B.F., Neubauer, R., Reich, R., Wenzel, T., Parsapoor, A. and Markl, G. (2018) The petrology of the Kaiserstuhl volcanic complex, SW Germany: The importance of metasomatized and oxidized lithospheric mantle for carbonatite generation. Journal of Petrology, 59, 1731-1762.

Carlson, E.T. (1956) Hydrogarnet formation in the system lime-alumina-silica-water. Journal of Research of the National Bureau of Standards, 56, 327-335.

Chakhmouradian, A.R. and McCammon, C.A. (2005) Schorlomite: a discussion of the crystal chemistry, formula, and inter-species boundaries. Physics and Chemistry of Minerals, 32, 277-289.

Cho, H. and Rossman, G.R. (1993) Single-crystal NMR studies of low-concentration hydrous species in minerals: Grossular garnet. American Mineralogist, 78, 1149-1164.

Dilnesa, B.Z., Lothenbach, B., Renaudin, G., Wichser, A., and Kulik, D. (2014) Synthesis and characrterization of $Ca_3(Al_xFe_{1-x})_2(SiO_4)_y(OH)_{4(3-y)}$. Cement and Concrete Research, 59, 96-111.

Flint, E.P. and Wells, L.S. (1941) Relationship of the garnet-hydrogarnet series to the sulfate resistance of portland cement. Journal of Research of the National Bureau of Standards, RP 1411, 27, 171-180.

Flint, E.P., McMurdie, H.F., and Wells, L.S. (1941) Hydrothermal and X-ray studies of the garnet-hydrogarnet series and the relationship of the series to hydration products of portland cement. National Bureau of Standards, Research, 26, Paper RP 1335, 13-33.

Geiger, C.A. and Armbruster, T. (1997) $Mn_3Al_2Si_3O_{12}$ spessartine and $Ca_3Al_2Si_3O_{12}$ grossular garnet: dynamical structural and thermodynamic properties. American Mineralogist, 82, 740-747.

Geiger, C.A. and Brearley, A. (in prep) Almandine II: A theoretical analysis of point defects and defect reactions and mineralogical and petrological implications, European Journal of Mineralogy.

Geiger, C.A. and Rossman, G.R. (2018) IR spectroscopy and OH^- in silicate garnet: The long quest to document the hydrogarnet substitution. American Mineralogist, 103, 384-393.

Geiger, C.A. and Rossman, G.R. (in press) Nano-size hydrogarnet clusters and proton ordering in calcium silicate garnet: Part I. The quest to understand the nature of "water" in garnet continues. American Mineralogist.

Geiger, C.A. and Rossman, G.R. (submitted – 2019c) Pyrope from the Dora Maira Massif, Western Alps: Water in the hydrogrossular. Contribution to Mineralogy and Petrology.

640 Geiger, C.A. and Rossman, G.R. (in prep. - 2019d) Hydrogarnet clusters and proton ordering in
641 spessartine: The continuing quest to understand H_2O in garnet.
642 Geiger, C.A., Stahl, A., and Rossman, G.R. (2000) Single-crystal IR- and UV/ VIS-spectroscopic
643 measurements on transition-metal-bearing pyrope: The incorporation of hydroxide in
644 garnet. European Journal of Mineralogy, 12, 259-271.
645 Khomenko, V.M., Langer, K., Beran, A., Koch-Müller, M., Fehr, T. (1994) Titanium substitution
646 and OH-bearing defects in hydrothermally grown pyrope crystals. Physics and Chemistry
647 of Minerals, 20, 483-488.
648 Kobayashi, S., and Shoji, T. (1983) Infrared analysis of the grossular-hydrogrossular series.
649 Mineralogical Journal, 11, 331-343.
650 Kühberger, A., Fehr, T., Huckenholz, H.G., and Amthauer, G. (1989) Crystal chemistry of a
651 natural schorlomite and Ti-andradites synthesized at different oxygen fugacities. Physics
652 and Chemistry of Minerals, 16, 734-740.
653 Kurka, A., Blanchard, M. and Ingrin, J. (2005) Kinetics of hydrogen extraction and deuteration in
654 grossular. Mineralogical Magazine, 69, 359-371.
655 Lager, G.A., Armbruster, T., and Faber, G. (1987) Neutron and X-ray diffraction study of
656 hydrogarnet $Ca_3Al_2(O_4H_4)_3$. American Mineralogist. 72, 756-765.
657 Libowitzky, E. and Rossman, G.R. (1997) An IR absorption calibration for water in minerals.
658 American Mineralogist, 82, 111-1115.
659 Locock, A.J. (2008) An Excel spreadsheet to recast analyses of garnet into end-member
660 components, and a synopsis of the crystal chemistry of natural silicate garnets. Computers
661 and Geosciences, 34, 1769-1780.
662 Locock, A., Luth, R.W., Cavell, R.G., Smith, D.G.W., and Duke, M.J.M. (1995) Spectroscopy of
663 the cation distribution in the schorlomite species of garnet. American Mineralogist, 80, 27-
664 38.
665 Lu, R. and Keppler, H. (1997) Water solubility in pyrope up to 100 kbar. Contributions to
666 Mineralogy and Petrology, 129, 35-42.

667 Maldener, J., Hösch, A., Langer, K., and Rauch, F. (2003) Hydrogen in some natural garnets
668 studied by nuclear reaction analysis and vibrational spectroscopy. Physics and Chemistry
669 of Minerals, 30, 337-344.
670 Normand, C. and William-Jones, A.E. (2007) Physicochemical conditions and timing of rodingite
671 formation: evidence from rodingite-hosted fluid inclusions in the JM Asbestos mine,
672 Asbestos, Québec. Geochemical Transactions, 8.11, 1-19.
673 Palke, A.C., Stebbins, J.F., Geiger, C.A., and Tippelt, G. (2015) Cation order-disorder in Fe-
674 bearing pyrope and grossular garnets: An ^{27}Al and ^{29}Si MAS NMR and ^{57}Fe Mössbauer
675 spectroscopy study. American Mineralogist, 100, 536-547.
676 Phichaikamjornwut, B., Skogby, H., Ounchanum, P., Limtrakun, P., and Boonsoong, A. (2011)
677 Hydrous components of grossular-andradite garnets from Thailand: thermal stability and
678 exchange kinetics. European Journal of Mineralogy, 24, 107-121.
679 Pistorius, C.W.F.T and Kennedy, G.C. (1960) Stability relations of grossularite and
680 hydrogrossularite at high temperatures and pressures. American Journal of Science, 258,
681 247-257.
682 Reynes, J., Jollands, M., Hermann, J., and Ireland (2018) Experimental constraints on hydrogen
683 diffusion in garnet. Contributions to Mineralogy and Petrology, 173, 23 p.
684 Rivas-Mercury, J.M., Pena, P., de Aza, A.H., and Turrillas, X. (2008) Dehydration of
685 $Ca_3Al_2(SiO_4)_y(OH)_{4(3-y)}$ ($0 < y < 0.176$) studied by neutron thermodiffractometry. Journal
686 of the European Ceramic Society, 28, 1737-1748.
687 Rossman, G.R. (2006) Analytical methods for measuring water in nominally anhydrous minerals.
688 Reviews in Mineralogy and Geochemistry. Eds., Keppler, H. and Smyth, J.R., v. 62, 1-28.
689 Mineralogical Society of America.
690 Rossman, G.R. and Aines, R.D. (1986) Spectroscopy of a birefringent grossular from Asbestos,
691 Quebec, Canada. American Mineralogist, 71, 779-780.
692 Rossman, G.R. and Aines, R.D. (1991) The hydrous components in garnets: Grossular-
693 hydrogrossular. American Mineralogist, 76, 1153-1164.

694 Schingaro, E., Lacalamita, M., Mesto, E., Ventruti, G., Pedrazzi, G., Ottolini, L., and Scordari, F.
695 (2016) Crystal chemistry and light elements analysis of Ti-rich garnets. American
696 Mineralogist, 101, 371-384.
697 Schmitt, A.C., Tokuda, M., Yoshiasa, A., and Nishiyama, T. (2019) Titanian andradite in the
698 Nomo rodingite: Chemistry, crystallography, and reaction relations. Journal of
699 Mineralogical and Petrological Sciences, 114, 111-121.
700 Shannon, R.D. (1976) Revised effective ionic radii and systematic studies of interatomic distances
701 in halides and chalcogenides. Acta Crystallographica, A32, 751-767.
702 Shannon, R.D. and Rossman, G.R. (1992) Dielectric constants of silicate garnets and the oxide
703 additivity rule. American Mineralogist, 77, 94-100.
704 Yoder, H.S., Jr. (1950) Stability relations of grossularite. The Journal of Geology, 58, 221-253.
705 Wright, K., Freer, R., and Catlow, C.R.A. (1994) The energetics and structure of the hydrogarnet
706 defect in grossular: A computer simulation study. Physics and Chemistry of Minerals, 20,
707 500-503.
708 Zhang, P., Ingrin, J., Depecker, C., and Xia, Q. (2015) Kinetics of deuteration in andradite and
709 garnet. American Mineralogist, 100, 1400-1410.

This is a preprint, the final version is subject to change, of the American Mineralogist (MSA)
Cite as Authors (Year) Title. American Mineralogist, in press.
DOI: https://doi.org/10.2138/am-2020-7257

710 Table 1. Description of natural garnet samples of GRR and their water concentrations and approximate compositions.

Garnet & Sample Label	Locality (Source)	Sample Description	Wt. % H_2O	Approximate Composition
Ti-bearing andradite GRR 3554	Magnet Cove, AR, USA (J. Zigras, Avant Mining, CIT-15810)	0.456 mm, "melanite variety", black	0.02	Ti-bearing andradite
Grossular GRR 946	Auerbach, Germany (G. Amthauer, Salzburg)	0.278 mm, both Fe^{2+} and Fe^{3+} present, brownish-pink; Rossman and Aines (1991)	0.13	Gross87Andr13
Grossular GRR 1411	Munam, Whanghedo, N. Korea (Y. Takeuchi, Univ. Tokyo, catalog UMUTMI-20124)	0.358 mm, skarn, greyish yellow-green, birefringent; Rossman and Aines (1991)	0.05	Gross65Andr35
Grossular GRR 1422	Wakefield, Ontario, Canada (CIT-12178)	0.509 mm, light yellow green; Rossman and Aines (1991)	0.01	Gross95Andr05
Grossular GRR 1424	Garnet Queen Mine?, Santa Rosa Mtns., CA, USA (CIT-8804)	0.518 mm, light brownish yellow; Rossman and Aines (1991)	0.09	Gross78Andr22
Grossular GRR 1429	Essex County, NY, USA (G. Novak – GN II-5)	0.255 mm, orange-brown; Novak and Gibbs (1971); Rossman and Aines (1991)	0.02	Gross78Andr22

This is a preprint, the final version is subject to change, of the American Mineralogist (MSA)
Cite as Authors (Year) Title. American Mineralogist, in press.
DOI: https://doi.org/10.2138/am-2020-7257

Grossular GRR 53	Asbestos, Quebec, Canada (CIT Collection #11240)	0.405 mm, light orange; Rossman and Aines (1986); Rossman and Aines (1991)	0.12	Gross94Andr06
Grossular GRR53b	Asbestos, Quebec, Canada	0.139 mm, light orange, isotropic; Rossman and Aines (1986)	0.10	Gross94Andr06
Grossular GRR 1038 C/R	Asbestos, Quebec, Canada (Rock H. Currier, Jewel Tunnel Imports)	0.276 mm, near colorless rim, vivid green core (Cr^{3+}); Rossman and Aines (1991)	0.08(0.05)*/0.21	Gross96Andr04
Grossular GRR 1285 NMR	Jeffrey Mine, Asbestos, Quebec, Canada (F. Allen)	0.030 mm; light orangish pink; Cho & Rossman (1993); Allen and Buseck (1998)	0.12	Gross98Andr02
Grossular GRR 1537	Jeffrey Mine, Asbestos, Quebec, Canada (R.D. Shannon, Dupont)	0.073 mm, colorless; Shannon and Rossman (1992)	0.19	Gross99Andr01
Grossular GRR 1538	Jeffrey Mine, Asbestos, Quebec, Canada (R.D. Shannon, Dupont)	0.173 mm, pale orangish pink, variety hessonite; Shannon and Rossman (1992)	0.23	Gross95Andr05

711 *Rim H_2O using all OH modes and (only hydrogrossular related bands).

This is a preprint, the final version is subject to change, of the American Mineralogist (MSA)
Cite as Authors (Year) Title. American Mineralogist, in press.
DOI: https://doi.org/10.2138/am-2020-7257

718 Table 3. Energies of OH^- stretching modes (greater than 3560 cm^{-1}) for various garnets at room temperature, their assignments and cluster type (see Part I -
719 Figure 4).

Various Natural Grossulars[§] (cm^{-1})	Synthetic Grossular[§] (cm^{-1})	Synthetic/Natural Andradite[#] (cm^{-1})	Synthetic Schorlomite[+]	Natural Ti-bearing Andradite* (cm^{-1})	Assignment & Cluster Type	Crystal Chemistry Cluster Type
3684-3688	~3688	-	-	-	Hydrous inclusion phase?	No cluster
3674-3678	-	-	-	-	Hydrous inclusion phase?	No cluster
~3660	~3666	-	-	~3664	Finite-size katoite cluster	Fig. 4a
~3657	~3660	-	-	~3654	Six $(H_4O_4)^{4-}$ Hydrogrossular cluster(?)	Fig. 4g
~3641	~3645	-	-	~3647	Five $(H_4O_4)^{4-}$ Hydrogrossular cluster	Fig. 4f
~3634	~3633	-	-	~3639	Four $(H_4O_4)^{4-}$ Hydrogrossular cluster	Fig. 4e
~3622	~3623	-	-	~3626	Three $(H_4O_4)^{4-}$ Hydrogrossular cluster	Fig. 4d
~3612	~3613	-	-	~3616	Two $(H_4O_4)^{4-}$ Hydrogrossular cluster	Fig. 4c
~3599	~3604	-	-	~3603	One $(H_4O_4)^{4-}$ Hydrogrossular cluster	Fig. 4b
-	-	~3611	-	-	Finite-size $Ca_3Fe^{3+}{}_2O_{12}H_{12}$ cluster(?)	Fig. 4a
~(3594)	-	-	-	~3589	Unspecified Hydroandradite cluster	?
~(3581)	~(3579)	-	-	~3577	Unspecified Hydroandradite cluster	?
~(3563)	~(3560)	~3563	~3568	~3560	One $(H_4O_4)^{4-}$ Hydroandradite cluster	Fig. 4b

720 [§]Part I this study, [#]Geiger and Rossman (2018) and Part I of this study, [+]Kühberger et al. (1989), *Sample HILDA 1 (Armbruster et al. 1998).

723
724 **FIGURES**

725

726 Figure 1. IR single-crystal spectrum in the energy range of the OH^- stretching vibrations at RT for a
727 magmatic Ti-bearing andradite (Table 1 - GRR 3554) from Magnet Cove, Arkansas, USA.

728

729 Figure 2. IR single-crystal spectrum in the energy range of the OH^- stretching vibrations at RT for Ti-
730 bearing andradite HILDA 1 (Armbruster et al. 1998) occurring in a chlorite schist from
731 Hildenkreuzjoch, Pfitschtal, South Tyrol, Italy. The fitted spectrum is shown below.

732

733 Figure 3. Stacked plot of IR spectra of different Ti-bearing garnets, andradite and schorlomite with the
734 spectra normalized to 1 mm crystal thickness. Some of the spectra have been slightly smoothed to
735 reduce minor spectral noise related to high-energy vibrations arising from water vapor in the IR
736 measuring chamber. Vertical green lines at a = 3656, b = 3638 and c = 3604 cm^{-1} give OH^- bands
737 representing the most abundant hydrogrossular clusters and the pink-brown lines at d = 3590, e =
738 3578 and f = 3561 cm^{-1} hydroandradite-like clusters. Calculated H_2O contents for the various garnets
739 in wt. % are: ZER1 12 = 0.35, HILDA 1 = 0.27, MUREIA (rim) 7 = 0.04, NZALA = 0.03, GRR 3554
740 = 0.02 and KAlS = 0.01.

741

742 Figure 4. Stacked plot of spectra for different grossular crystals (Table 1) with the spectra normalized
743 to 1 mm crystal thickness. Vertical green lines at a = 3657, b = 3641 and c = 3599 cm^{-1} give OH^-
744 modes representing various hydrogrossular-like clusters and pink-brown lines at d = 3584 and e =
745 3566 cm^{-1} various hydroandradite-like clusters.

746

747 Figure 5. Stacked plot of spectra for different grossular crystals (Table 1) from Asbestos, Quebec,
748 Canada with the spectra normalized to 1 mm crystal thickness. “R” means crystal rim and “C” means
749 crystal core. Vertical lines define various OH^- peak positions in wavenumbers (cm^{-1}) with a = 3664, b
750 = 3657, c = 3641, d = 3633, e = 3622, f = 3612, g = 3601, h = 3583, i = 3560, and where the green

lines represent various hydrogrossular-like clusters and pink-brown lines various hydroandradite-like clusters.

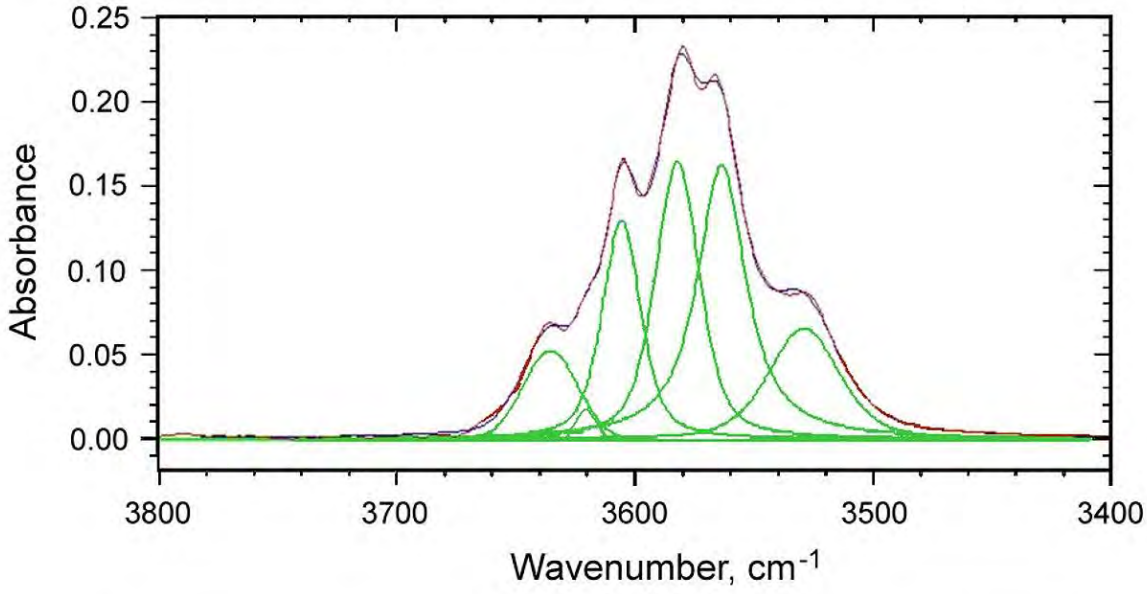

Curve Name	Centre	Width	Height	% Gaussian	Type	Area
Curve 1	3529	35.4	0.07	58	Mixed	3.0
Curve 2	3563	24.6	0.16	10	Mixed	6.2
Curve 3	3582	22.2	0.17	50	Mixed	4.8
Curve 4	3606	19.2	0.13	47	Mixed	3.4
Curve 5	3635	27.2	0.05	100	Mixed	1.5
Curve 6	3620	9.06	0.02	100	Mixed	0.2

Figure 1.

This is a preprint, the final version is subject to change, of the American Mineralogist (MSA)
Cite as Authors (Year) Title. American Mineralogist, in press.
DOI: https://doi.org/10.2138/am-2020-7257

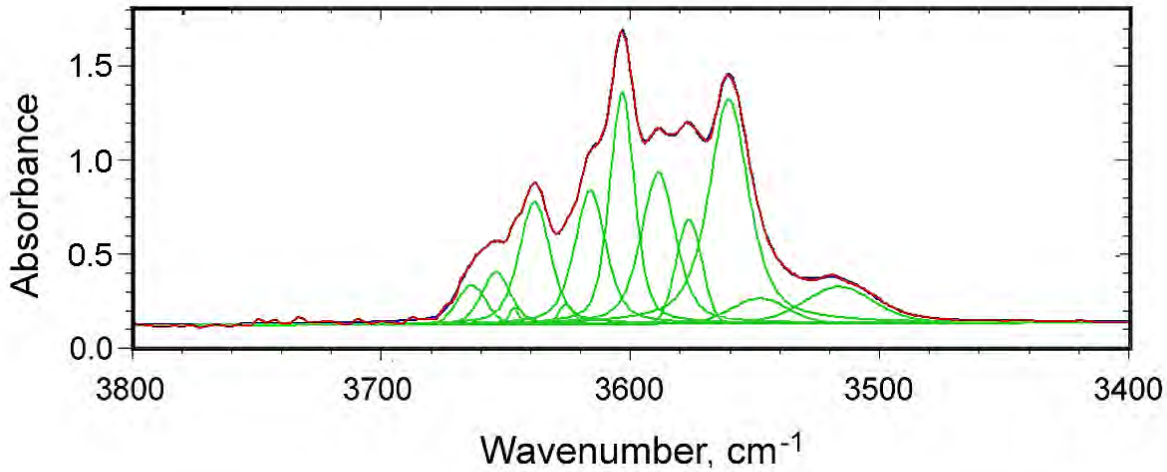

Curve Name	Centre	Width	Height	% Gaussian	Type	Area
Curve 1	3516	33.4	0.20	76	Mixed	7.8
Curve 2	3664	13.9	0.21	100	Mixed	3.1
Curve 3	3654	13.6	0.28	62	Mixed	4.8
Curve 4	3647	4.5	0.09	38	Mixed	0.6
Curve 5	3639	14.7	0.66	54	Mixed	12.5
Curve 6	3626	6.8	0.11	72	Mixed	0.9
Curve 7	3616	14.9	0.72	49	Mixed	14.1
Curve 8	3603	11.7	1.24	55	Mixed	18.7
Curve 9	3589	16.4	0.81	51	Mixed	17.4
Curve 10	3576	12.2	0.56	100	Mixed	7.2
Curve 11	3560	19.0	1.20	35	Mixed	31.8
Curve 12	3548	26.7	0.14	100	Mixed	3.9

788

789

790

791 Figure 2.

792

793

794

This is a preprint, the final version is subject to change, of the American Mineralogist (MSA)
Cite as Authors (Year) Title. American Mineralogist, in press.
DOI: https://doi.org/10.2138/am-2020-7257

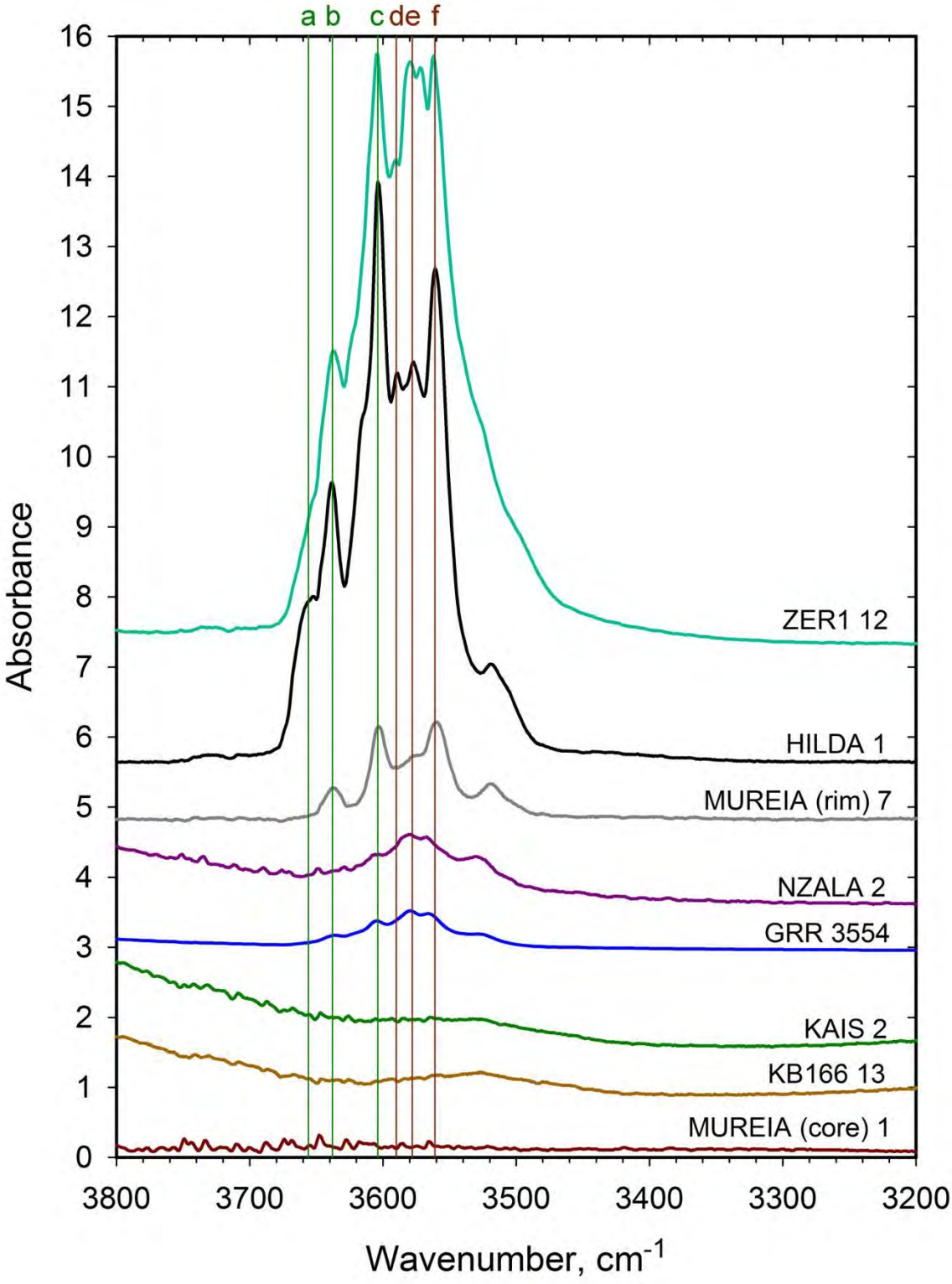

795

796

797

798 Figure 3.

799

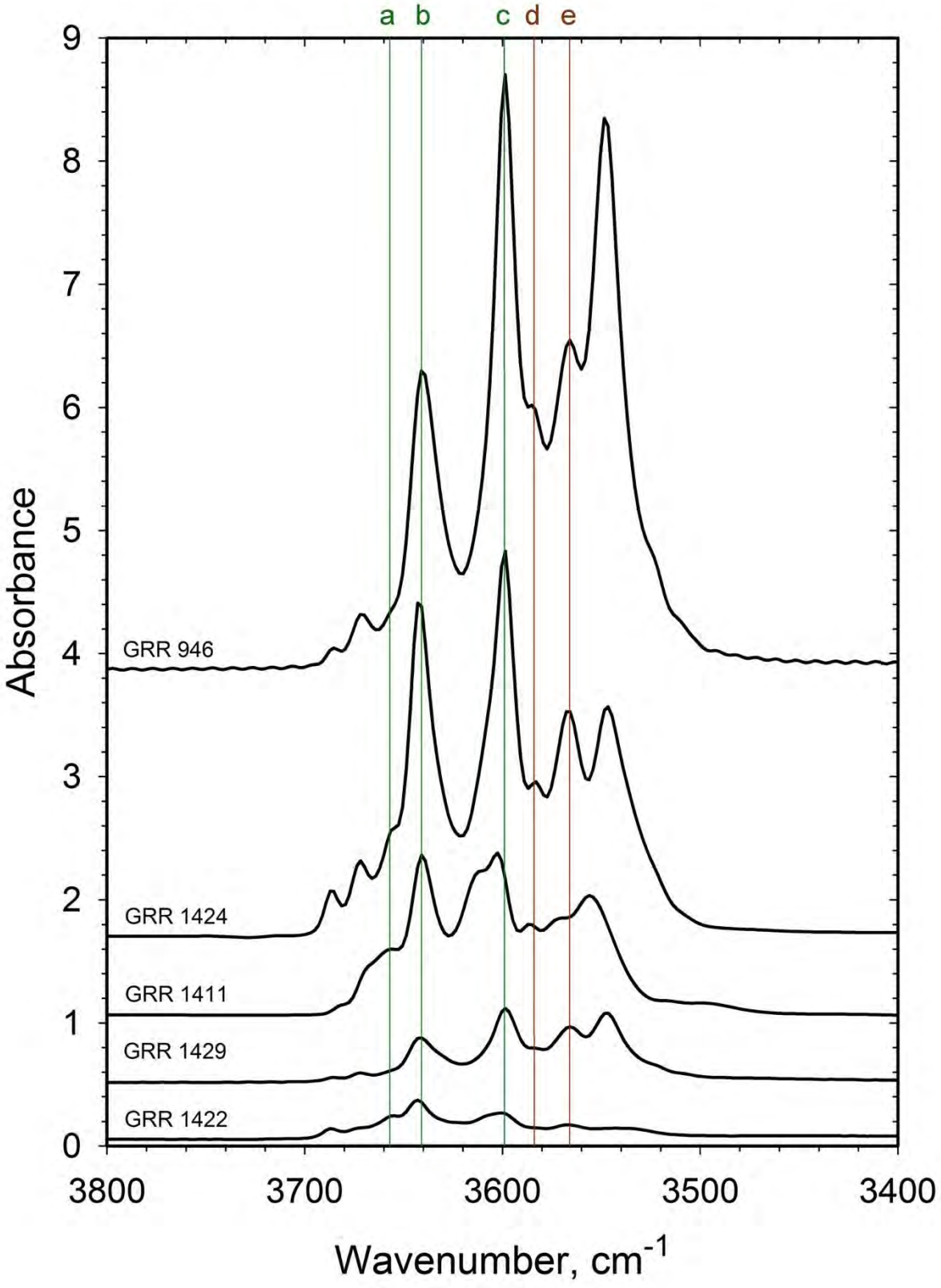

800

801

802 Figure 4.

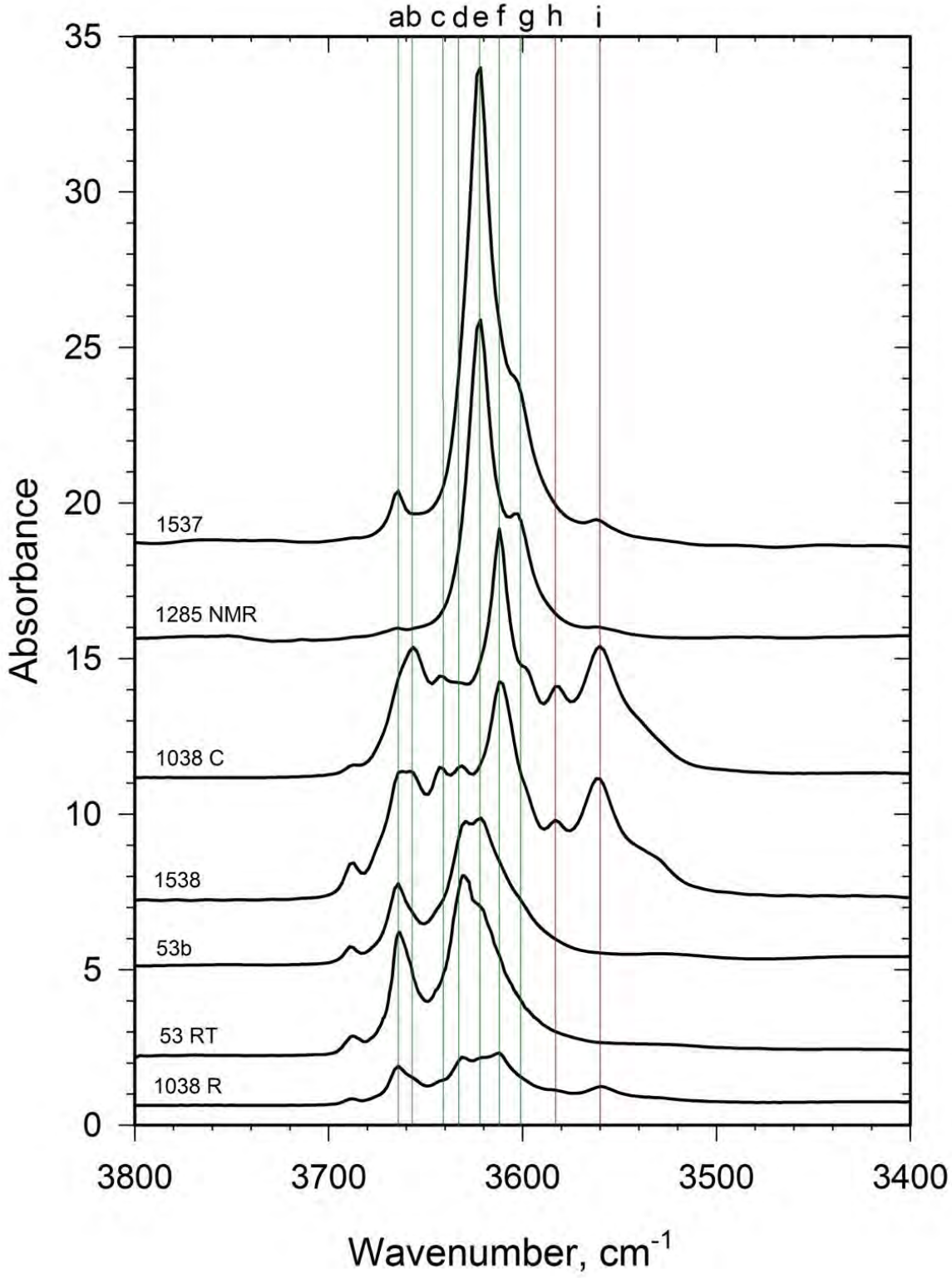

803

804

805

806 Figure 5.